Effect of Nanoscopic Particles on the Mesophase Structure of Diblock Copolymers

Jae Youn Lee,[†] Russell B. Thompson,[†] David Jasnow,[‡] and Anna C. Balazs*,[†]

Chemical Engineering Department, University of Pittsburgh, Pittsburgh, Pennsylvania 15261; and Department of Physics and Astronomy, University of Pittsburgh, Pittsburgh, Pennsylvania 15260

Introduction. The fabrication of novel biomimetic[1] photonic[2] and electronic[3] materials requires the manipulation of both organic and inorganic materials at the nanometer length scale. One possible means of achieving this level of control is to add inorganic nanoparticles to a melt of diblock copolymers.[4] The microphase separation of the copolymers into nanoscopic, ordered domains could be harnessed to "template" the organization of the particles into nanoplanes, -wires, or -spheres within the polymer matrix.[5] However, as we show below, the particles are not passive and can affect the overall morphology of the mixture. We also show that this effect is sufficiently robust that it can be found in both the strong and intermediate segregation limits of the diblock melts (i.e., both low and intermediate temperatures).

To probe the low-temperature behavior of the system, we adapt our recent strong segregation scaling theory (SST) for mixtures of AB diblocks and spherical particles.[6] We previously investigated the case in which the particles have a strong affinity for the A blocks and thus are preferentially localized in the A domains.[6] We now generalize the theory to allow the particles to interact with both the A and B blocks and subsequently find that variations in the particle−block interaction energies can induce phase transitions in the morphology of the mixture. At fixed interactions, variations in particle size can also induce similar transitions.

To investigate the behavior of the system at intermediate temperature ranges and demonstrate the generality of our findings, we turn to our recently developed theory[5] that combines a self-consistent field theory (SCFT) for the polymers with a density functional theory (DFT) for the particles. The SCFT used in our approach can accurately capture the behavior of block copolymers in both the weak and intermediate segregation limits[7−9] and remains the method of choice for a numerical analysis of the potential equilibrium phases. In previous SCFT/DFT studies,[5] we focused on cases where the particles are preferentially localized in the A phase of an AB diblock. In this paper, we vary the particles' solubility within the blocks and find, in accordance with our new scaling results, that variations in the particle interaction energies or size can induce transitions between the different periodic mesophases formed by the system. Using both methods, we generate phase diagrams to pinpoint the conditions that give rise to such structural transitions. The findings provide new guidelines for controlling the spatial organization of organic/inorganic hybrid materials.

[†] Chemical Engineering Department, University of Pittsburgh.
[‡] Department of Physics and Astronomy, University of Pittsburgh.

The Models. The polymer/particle mixture consists of a volume fraction ϕ_p of solid spherical particles of radius R_p and a volume fraction $(1 - \phi_p)$ of molten AB diblocks. Each diblock consists of N segments, each of volume ρ_0^{-1}. The fraction of A segments per chain is denoted by f. The enthalpic interaction between an A segment and a B segment is described by the dimensionless Flory−Huggins parameter, χ_{AB}. The parameters χ_{AP} and χ_{BP} describe the enthalpic interactions between the particles and the respective blocks. As a function of $(\chi_{AB}N)$ and f, the pure diblock melt can form a variety of spatially periodic microstructures. Here, we restrict our attention to the three "classical" morphologies, lamellar, cylindrical, and spherical, and neglect the bicontinuous phases [10−13] that exist only in narrow ranges of composition.

Within our scaling theory (SST), we assume that the system is in the low-temperature limit where $\chi_{AB}N \gg 10$. Here, the A blocks and B blocks are highly stretched and interfacial regions separating the A and B domains are very narrow.[14] In our previous SST model,[6] we assumed that $\chi_{AP} = 0$ and $\chi_{AB} = \chi_{BP}$; thus, the particles were chemically identical to, or effectively coated by, the A species. In the present model, we allow both χ_{AP} and χ_{BP} to vary and, hence, can model particles that are chemically distinct from A. Furthermore, the particles are now distributed in both the A and B regions, not just in the A region, as in the previous study.[6] For simplicity, we assume the particles to be uniformly distributed within the respective domains. We let the variable X represent the fraction of particles in the A phase and $(1 - X)$ equal the fraction in the B phase. The assumption that the particles are uniformly distributed is reasonable for relatively low volume fractions of particles. At higher volume fractions, we observed[5,6] that, even if the spheres are compatible with the blocks, large particles will segregate within the domains and thus reduce the entropic penalty associated with the chains stretching to get around the solids.

To describe the ordered phases, we must specify the local volume fraction of particles in the A domains, $\psi_A = (\phi_p X/(\phi_p X + f(1 - \phi_p)))$, and the local volume fraction of particles in the B domains, $\psi_B = (\phi_p(1 - X)/(\phi_p(1 - X) + (1 - f)(1 - \phi_p)))$. Within strong segregation theory for the ordered phases, the free energy density contribution due to the particles can be written as[6]

$$g_{part} = (\phi_p R_0^3/(V_p N^{3/2})) [X\ln(\psi_A) + (1 - X) \times \ln(\psi_B) + X\Psi_{CS}(\psi_A) + (1 - X)\Psi_{CS}(\psi_B) + XR_p^2/4R_0^2 f a_0^2 + (1 - X)R_p^2/4R_0^2(1 - f)a_0^2] + \chi_{AP}N^{-3/2}(1 - \psi_A)\psi_A(R_0/(2N^{1/2}R_p)) + \chi_{BP}N^{-3/2}(1 - \psi_B)\psi_B(R_0/(2N^{1/2}R_p)) \quad (1)$$

where $R_0 \equiv aN^{1/2}$ is the characteristic size of the polymer and a is the statistical segment length, which is assumed to be the same for both the A and B segments. The volume of the particle is $V_p = (4\pi/3)R_p^3$ and $a_0 = 1/\sqrt{6}$. The first two terms on the right-hand side (rhs) of eq 1 represent the ideal part of the translational entropy of the particles in the A and B domains, respectively. The nonideal part of the translational entropy of the hard spheres is approximated by the

Carnahan−Starling equation,[15] $\Psi_{CS}(\psi_i) = (4\psi_i - 3\psi_i^2)/(1 - \psi_i)^2$, where i is A or B and ψ_i is defined above. The next two terms on the rhs of eq 1 describe the additional free energy loss incurred by each block due to the stretching in the "transverse" direction that is required to get around the particles.[6] Finally, the last two terms are the enthaplic terms that describe the particle−polymer interactions; the expression is normalized so that for $R_p = R_0/(2N^{1/2})$ the system describes diblocks in a solvent.

The polymer contribution to the free energy of the ordered phases is given by[6]

$$g_{poly} = N^{-3/2} [((1 - \phi_p)/N) \ln(1 - \phi_p) + 3(1 - \phi_p)^{2/3}\chi_{AB}^{1/3}(2N)^{-2/3}\lambda^{2/3}\kappa^{1/3}] \quad (2)$$

The first term on the rhs describes the translational entropy of the polymers and the second term arises from the elastic energy of the chains and the interfacial tension between the different domains.[16] The prefactors κ and λ depend on the specific morphology (lamellar, cylindrical, or spherical), the nature of the majority phase (A or B), the particle density ϕ_p, the diblock composition f,[6,14] and ψ_A and ψ_B.

To calculate the phase diagram, we sum eqs 1 and 2 and minimize with respect to X for each ϕ_p and f and for each possible structure. The result of such minimization gives us the map of the lowest-energy ordered phases. To complete the phase diagram, we must compare these free energies with that of the disordered phase.

In the disordered phase, both particles and diblocks are dispersed uniformly in space. Thus, the free energy is modified to yield:

$$g_{dis} = (\phi_p R_0^3/(V_p N^{3/2})) [\ln(\phi_p) + \Psi_{CS}(\phi_p) + (1 - \phi_p)R_p^2/4R_0^2 a_0^2] + \chi_{AP}N^{-3/2}f(1 - \phi_p)\phi_p(R_0/(2N^{1/2}R_p)) + \chi_{BP}N^{-3/2}(1 - f)(1 - \phi_p)\phi_p(R_0/(2N^{1/2}R_p)) + N^{-3/2}((1 - \phi_p)/N) \ln(1 - \phi_p) + \chi_{AB}N^{-3/2}f(1 - \phi_p)^2(1 - f) \quad (3)$$

Within this strong segregation approximation, we can calculate phase diagrams as a function of particle size and the various χ's.

In this study, we also employ our hybrid SCFT/DFT model[5] for polymer/particle mixtures. The SCFT/DFT constitutes a powerful method for determining the phase behavior of the system since we are not constrained to make a priori assumptions about the structure of the phase or the distribution of particles. In SCF theory, pairwise interactions between differing segments are replaced by the interaction of each segment with the average field created by the other segments. Here, we let $w_A(\mathbf{r})$ denote the value at a point $\mathbf{r}$ of the mean field felt by the A segments, $w_B(\mathbf{r})$ denote the field for B segments, and $w_p(\mathbf{r})$ represent the field for particles. Using this approach, the free energy for our system is given by $F_T = F_e + F_d + F_p$. The first term, F_e, details the enthalpic interactions:

$$F_e = (1/V) \int d\mathbf{r} [\chi_{AB}N\varphi_A(\mathbf{r})\varphi_B(\mathbf{r}) + \chi_{BP}N\varphi_B(\mathbf{r})\varphi_P(\mathbf{r}) + \chi_{AP}N\varphi_A(\mathbf{r})\varphi_P(\mathbf{r})] \quad (4)$$

where V is the volume of the system and $\varphi_A(\mathbf{r})$, $\varphi_B(\mathbf{r})$, and $\varphi_P(\mathbf{r})$ are the local concentrations of A segments, B segments, and particles, respectively. The diblock entropic free energy F_d is[17]

$$F_d = (1 - \phi_P) \ln[V(1 - \phi_P)/Q_d] - (1/V) \int d\mathbf{r} [w_A(\mathbf{r})\varphi_A(\mathbf{r}) + w_B(\mathbf{r})\varphi_B(\mathbf{r})] \quad (5)$$

where Q_d is the partition function of a single diblock subject to the fields $w_A(\mathbf{r})$ and $w_B(\mathbf{r})$. Finally, the particle entropic contributions to the free energy is given by

$$F_p = (\phi_P/\alpha) \ln(V\phi_P/Q_p\alpha) - (1/V) \int d\mathbf{r} [w_p(\mathbf{r})\rho_p(\mathbf{r})] + (1/V) \int d\mathbf{r} \rho_p(\mathbf{r})\Psi_{CS}[\bar{\varphi}_p(\mathbf{r})] \quad (6)$$

where Q_p is the partition function of a single particle subject to the field $w_p(\mathbf{r})$. The local particle volume fraction, $\varphi_p(\mathbf{r})$, is related to the dimensionless center of mass distribution, $\rho_p(\mathbf{r})$, by

$$\varphi_P(\mathbf{r}) = (4\alpha/(3\pi R_p^3)) \int_{|r'|<R} d\mathbf{r}' \rho_p(\mathbf{r} + \mathbf{r}') \quad (7)$$

The parameter $\alpha = (4\pi R_p^3\rho_0/(3 N))$ denotes the particle-to-diblock volume ratio. The last term of F_p describes the excess (nonideal) steric free energy of the particles through the DFT derived by Tarazona.[18,19] In particular, the Carnahan−Starling function for the excess free energy of a hard-sphere fluid, Ψ_{CS}, is now evaluated with the "weighted" (locally averaged) particle density, $\bar{\varphi}_p(\mathbf{r})$.[18]

In the SCFT, $w_A(\mathbf{r})$, $w_B(\mathbf{r})$, and $w_p(\mathbf{r})$ are determined by locating saddle points in the free energy functional F subject to the incompressibility constraint: $\varphi_A(\mathbf{r}) + \varphi_B(\mathbf{r}) + \varphi_P(\mathbf{r}) = 1$. This yields a system of equations that is solved numerically and self-consistently to give possible equilibrium solutions. To obtain these solutions, we implement the combinatorial screening technique of Drolet and Fredrickson.[20] We make an initial random guess for the fields and calculate all the densities and the free energy at each step; the fields are then recalculated and the entire process is repeated until changes in the diblock densities at each step become sufficiently small. In addition, we also minimize our free energy with respect to the size of the simulation box, as proposed by Bohbot-Raviv and Wang.[21]

Results and Discussion. Our aim is to determine how the preferential affinity of the particles for the A or B blocks and the size of the particles affect the phase behavior of various diblock/particle mixtures. To analyze these effects, we first calculated phase diagrams using the SST as a function of the particle interaction parameters for the entire range of the diblock compositions (i.e., values of f ranging from 0 to 1) and repeated these calculations for different particle sizes. In plots that were constructed with this SST, we fix $\chi_{AP} = 0$ and vary χ_{BP} to from −1 to +1, allowing us to investigate both cases $\chi_{AP} < \chi_{BP}$ and $\chi_{AP} > \chi_{BP}$. The values of the other variables are fixed at $N = 300$, $\phi_p = 0.15$, $\chi_{AB} = 1$. Figure 1 shows the plots calculated from the SST for the following cases: in part a, $R_p = 0.18R_0$ and in part b, $R_p = 0.06 R_0$.

Figure 1a illustrates the dramatic effects of varying χ_{BP} for the larger particles. Consider the point $f = 0.3$. An increase in χ_{BP} from −1 to +1 drives a transition from the cylindrical phase to the lamellar morphology. By increasing χ_{BP}, the particles are driven from the

$R_p = 0.18 R_0$

(a)

$R_p = 0.06 R_0$

(b)
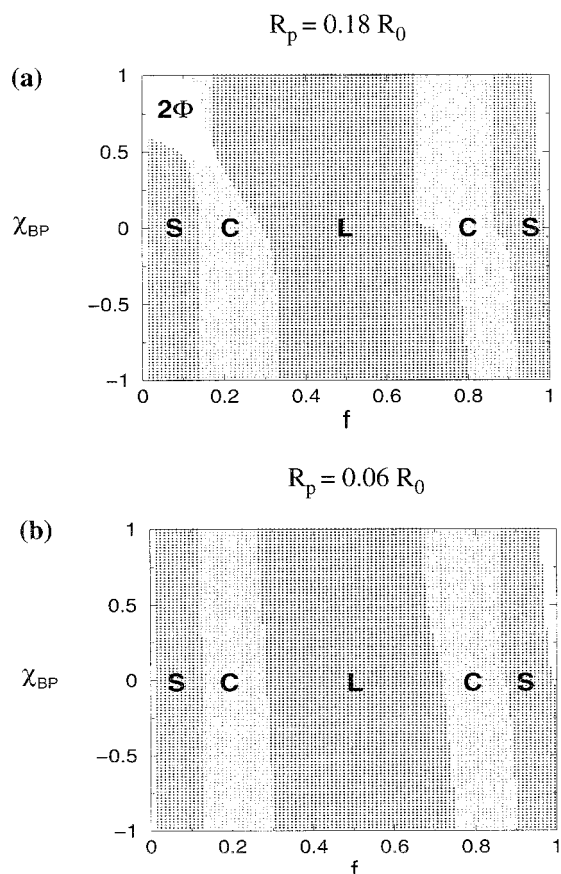
Figure 1. Phase diagrams obtained from the SST as a function of χ_{BP} and the block composition f. The following letters mark the different phases: spherical is denoted by (S), cylindrical by (C), and lamellar by (L). Two-phase regions (2Φ) are also shown. Here, $\chi_{AB} = 1$, $\chi_{AP} = 0$, $N = 300$, and $\phi_p = 0.15$ and in part a, $R_p = 0.18R_0$, and in part b, $R_p = 0.06R_0$.

unfavorable B domain, and enhance the effective A composition of the chains (f_{eff}), promoting the formation of the lamellar structure. Conversely, at $f = 0.75$, increasing χ_{BP} promotes a transition from the lamellar phase to the cylindrical structure. Again, increasing the effective repulsion between the B blocks and particles drives the spheres into the more favorable A domains, thereby increasing f_{eff} and promoting the formation of the cylindrical mesophase.

In Figure 1a, the phase boundaries between the lamellar and cylindrical regions display a pronounced sigmoidal shape. This effect is also present in Figure 1b, but to a much smaller extent. Consequently, at fixed f, χ_{AP}, and χ_{BP}, composites that exhibit one structure for the small particles can exhibit a different morphology for the larger particles. This can be seen, for example, by comparing parts a and b of Figure 1 at $f = 0.25$ and $\chi_{BP} = 0.75$; for small particles, the system is in the cylindrical phase, while the large particle system exhibits a lamellar structure.

To further evaluate and visualize the effect of particle size, we turn to the results of the SCFT/DFT calculations. We now fix $\bar{N} = 1000$, where $\bar{N} = \rho_0^2 a_0^6 N$ is the invariant polymerization index, (which corresponds to $N \approx 300$ using a and ρ_0 for polystyrene [22]) and set $\chi_{AB}N = 20$, placing our system in the intermediate segregation regime. In addition, $f = 0.35$ and $\phi_p = 0.15$. To emphasize the effect of particle size, we set $\chi_{AP} = \chi_{BP} = 0.02$ so the particles are nonselective. Figure 2 shows the density profiles for the A blocks and particles for

(a) $R_p = 0.1 R_0$

$R_p = 0.3 R_0$

(b)
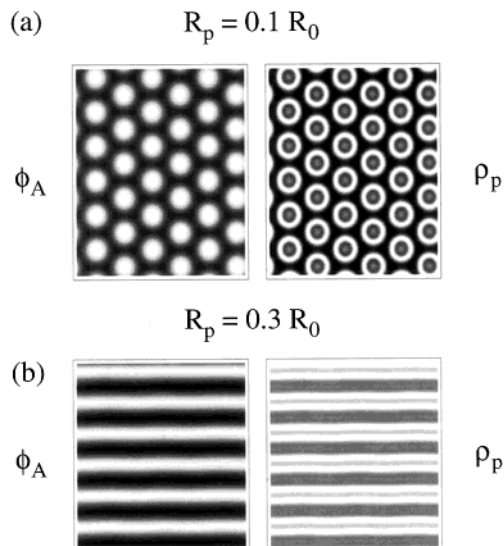
Figure 2. Two-dimensional density plots for the diblock/particle systems obtained from the SCFT/DFT theory. Plots are for $\chi_{AB}N = 20$, $\chi_{AP} = \chi_{BP} = 0.02$, $\bar{N} = 1000$, $f = 0.35$, and $\phi_p = 0.15$. Plots on the left represent the distribution of the A blocks and plots on the right represent the distribution of the centers of mass of the particles. Light regions indicate a high density, while dark regions indicate low densities. The image in part a shows that the system displays a cylindrical phase when $R_p = 0.1R_0$ and the image in part b shows that the mixture forms a lamellar phase when the particle size is increased to $R_p = 0.3R_0$.

two different particle sizes: $R_p = 0.1R_0$ and $R_p = 0.3R_0$. We observe a phase transition from the cylindrical morphology (Figure 2a) to the lamellar morphology (Figure 2b) as the particle radius is increased. This finding agrees qualitatively with our observations from the scaling theory. Associated with the observed phase transition is a significant shift in the particle distribution, as shown in Figure 3. Despite the nonselective block−particle interaction, the particle concentration is much higher in the A domain for the larger particles than for the smaller particles. The small particles distribute more or less uniformly over both the A and B domains, with a slightly higher concentration at the AB interface. This latter observation coincides with theoretical predictions for the behavior of a neutral solvent added to diblock copolymers.[23,24] The small excess of the $R_p = 0.1R_0$ particles at the interface is presumably driven by the enthalpic gain in reducing the interfacial tension, γ, between the A and B blocks. A closer look at the particle distributions reveals that the larger particles are mostly positioned at the AB interface, indicating that the enthalpic gain obtained from reducing γ wins over the loss of the particles' translational entropy. Plots of the particle center distributions (not shown here) reveal that large particles at the interface bulge out equally into both domains yet disproportionately expand each domain since the diblock is not symmetric (i.e., $f = 0.35$). As a result, the effective asymmetry in block composition diminishes, and hence promotes the phase transition from the cylindrical to the lamellar morphology.

To summarize our analysis of the effect of particle size and interaction energy on the phase boundaries, in Figure 4 we plot results from the SCFT/DFT that reveal the stable morphologies at fixed values of f, ϕ_p, χ_{AB}, and χ_{AP} for different values of R_p and χ_{BP}. Circles represent cylindrical morphologies and squares indicate lamellar structures. Qualitatively similar results are obtained in

(a)
$$R_p = 0.1 \, R_0$$

(b)
$$R_p = 0.3 \, R_0$$
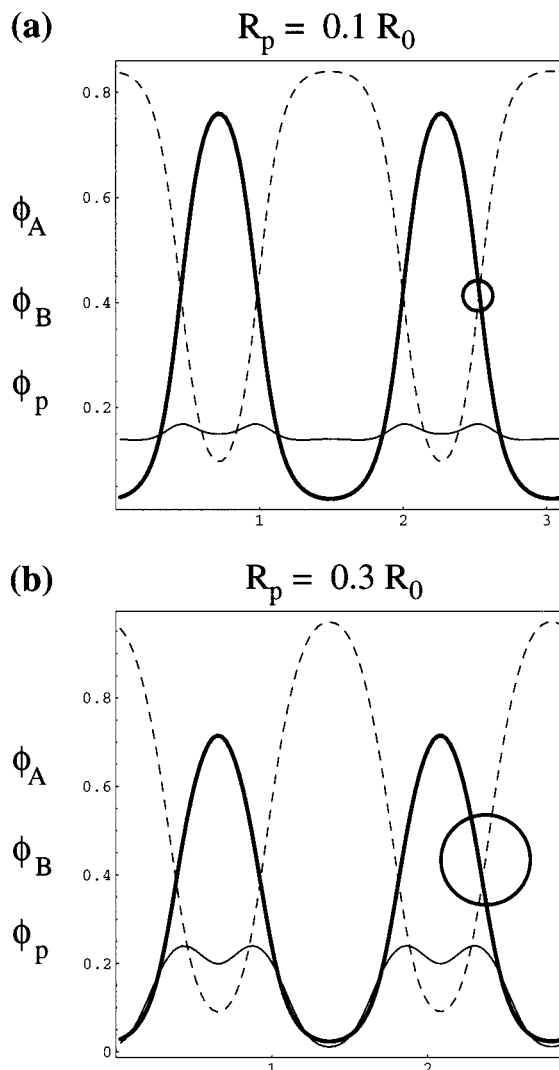
Figure 3. One-dimensional density profiles for diblock/particle systems obtained from the SCFT/DFT theory. The parameters are identical to those used in Figure 2. Solid lines represent ϕ_A, the dot—dashed lines mark ϕ_B, and the dashed lines represent ϕ_p. The circles placed at the interfaces indicate the size of the particles relative to the block domains.
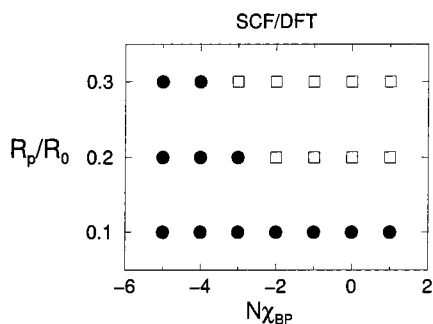
Figure 4. Equilibrium morphologies of diblock/particle systems are plotted as a function of the particle radius R_p and χ_{BP}. Calculations were performed with the SCFT/DFT theory. Filled circles represent cylindrical morphologies and squares indicate lamellar morphologies. Here, $\chi_{AB}N = 20$, $\chi_{AP} = 0$, $\bar{N} = 1000$, $f = 0.35$, and $\phi_p = 0.15$.

the low-temperature limit using the SST model. The plot in Figure 4 shows R_p and χ_{BP} dependent phase transitions that motivate the qualitative arguments presented above.

These results indicate that the morphologies of organic/inorganic hybrid materials can be tailored by adding particles of specific sizes and chemistry. The results also highlight the fact that in such complex mixtures, it is not simply that the ordering of the copolymers templates the spatial organization of the particles. The particle concentration is not a "passive scalar" and can affect the self-assembly of the chains. From knowledge of interactions in copolymer/particle mixtures, we can facilitate the fabrication of nanostructured composites with the desired morphologies and properties.

References and Notes

(1) Stupp, S. I.; Braun, P. V. *Science* **1997**, *277*, 1242.
(2) Fink, Y.; Urbas, A. M.; Bawendi, M. G.; Joannopoulos, J. D.; Thomas, E. L. *J. Lightwave Technol.* **1999**, *17*, 1963.
(3) Jeoung, E.; Galow, T. H.; Schotter, J.; Bal, M.; Ursache, A.; Tuominen, M. T.; Stafford, C. M.; Russell, T. P.; Rotello, V. M. *Langmuir* **2001**, *17*, 6396.
(4) See for example: (a) Lopes, W. A.; Jaeger, H. M. *Nature* **2001**, *414*, 735. (b) Lauter-Pasyuk, V. et al., *Physica B* **1997**, *241*, 1092. Lauter-Pasyuk, V. et al., *Physica B* **1998**, *248*, 243. Hamdoun, B. et al., *J. Phys. (Fr.) II* 1996, **1996**, *6*, 493. (c) Krishnamoorti, R.; Silva, A. S.; Mitchell, C. A. *J. Chem. Phys.* **2001**, *115*, 7175.
(5) (a) Thompson, R. B.; Ginzburg, V. V.; Matsen, M. W.; Balazs, A. C. *Science* **2001**, *292*, 2469. (b) Thompson, R. B.; Ginzburg, V. V.; Matsen, M. W.; Balazs, A. C. *Macromolecules* **2002**, *35*, 1060.
(6) Huh, J.; Ginzburg, V. V.; Balazs, A. C. *Macromolecules* **2000**, *33*, 8085.
(7) Matsen, M. W. *J. Phys.: Condens. Matter* **2002**, *14*, R21 and references therein.
(8) We note that numerical differences do exist between SST and SCFT for the behavior of pure diblock melts at low temperatures. Recently Matsen[9] modified the implementation of the SCFT to readily extend the model to the strong segregation limit. A comparison of this SCFT to various SST models still suggests a quantitative discrepancy between the two approaches. A more detailed discussion of this point is given in ref 9.
(9) Matsen, M. W. *J. Chem. Phys.* **2001**, *114*, 10528.
(10) Matsen, M. W.; Schick, M. *Phys. Rev. Lett.* **1994**, *72*, 2660.
(11) Hajduk, D. A.; Harper, P. E.; Gruner, S. M.; Honeker, C. C.; Kim, G.; Thomas, E. L.; Fetters, L. J. *Macromolecules* **1994**, *27*, 4075.
(12) Olmsted, P. D.; Milner, S. T. *Phys. Rev. Lett.* **1994**, *72*, 936.
(13) Xi, H.; Milner, S. T. *Macromolecules* **1996**, *29*, 2404.
(14) Semenov, A. N. *Sov. Phys. JETP* **1985**, *61*, 733.
(15) Carnahan, N. F.; Starling, K. E. *J. Chem. Phys.* **1969**, *51*, 635.
(16) The dimensionless prefactor κ appears in the expression for the elastic part of the free energy for the chains (see ref 14). The dimensionless prefactor λ appears in the surface tension term. These two terms are added to the translational entropy of the chains to obtain the total free energy for the diblocks. Minimizing this total free energy expression with respect to the size of the Wigner-Seitz unit cell, we obtain the expression in eq 2. Further details are given in refs 6 and 14.
(17) Matsen, M. W.; Bates, F. S. *Macromolecules* **1996**, *29*, 1091.
(18) Tarazona, P. *Mol. Phys.* **1984**, *52*, 81.
(19) Vroege, G. J.; Lekkerkerker, H. N. W. *Rep. Prog. Phys.* **1992**, *55*, 1241.
(20) Drolet, F.; Fredrickson, G. H. *Phys. Rev. Lett.* **1999**, *83*, 4317.
(21) Bohbot-Raviv, Y.; Wang, Z.-G. *Phys. Rev. Lett.* **2000**, *85*, 3428.
(22) Banaszak, M.; Whitmore, M. D. *Macromolecules* **1992**, *25*, 3406.
(23) Whitmore, M. D.; Noolandi, J. *J. Chem. Phys.* **1990**, *93*, 2946.
(24) Hanley, K. J.; Lodge, T. P.; Huang, C.-I. *Macromolecules* **2000**, *33*, 5918. Huang, C.-I.; Lodge, T. P. *Macromolecules* **1998**, *31*, 3556.